

LASER INTERFEROMETER GRAVITATIONAL WAVE OBSERVATORY
- LIGO -
CALIFORNIA INSTITUTE OF TECHNOLOGY
MASSACHUSETTS INSTITUTE OF TECHNOLOGY

Technical Note	LIGO-T2000181-v2	2021/10/25
<h1>Nonlinear Regression of Technical Noise in LIGO with Machine Learning</h1>		
<p>Hang Yu, Zachary Mark, Rana X Adhikari <i>LIGO Laboratory, California Institute of Technology</i></p>		

California Institute of Technology
LIGO Project, MS 100-36
Pasadena, CA 91125
Phone (626) 395-2129
Fax (626) 304-9834
E-mail: info@ligo.caltech.edu

Massachusetts Institute of Technology
LIGO Project, Room NW22-295
Cambridge, MA 02139
Phone (617) 253-4824
Fax (617) 253-7014
E-mail: info@ligo.mit.edu

WWW: <http://www.ligo.caltech.edu/>

Contents

1	Introduction	3
2	Examples of Nonlinear Coupling Mechanisms	4
3	Noise regression with Neural Networks	5
4	Reinforcement Learning for Feedback Controls	6
A	Astrophysical Motivations	7

1 Introduction

Broadly speaking, the sensitivity of aLIGO is determined by two kinds of noise sources, an unsubtractable one and a subtractable one. The former originates from quantum or thermal fluctuations and shows up only in the main GW readout channel. It cannot be distinguished from the GW signal and thus sets a fundamental limit of the instrument's sensitivity. On the other hand, the latter one is due to cross-couplings from the auxiliary control loops and/or some environmental perturbations like the seismic motion. The perturbations causing excess noises in DARM are also continuously recorded in (tens of thousands of) auxiliary channels, and therefore can in principle be used to reconstruct and then clean up the contamination showing up in the main GW readout.

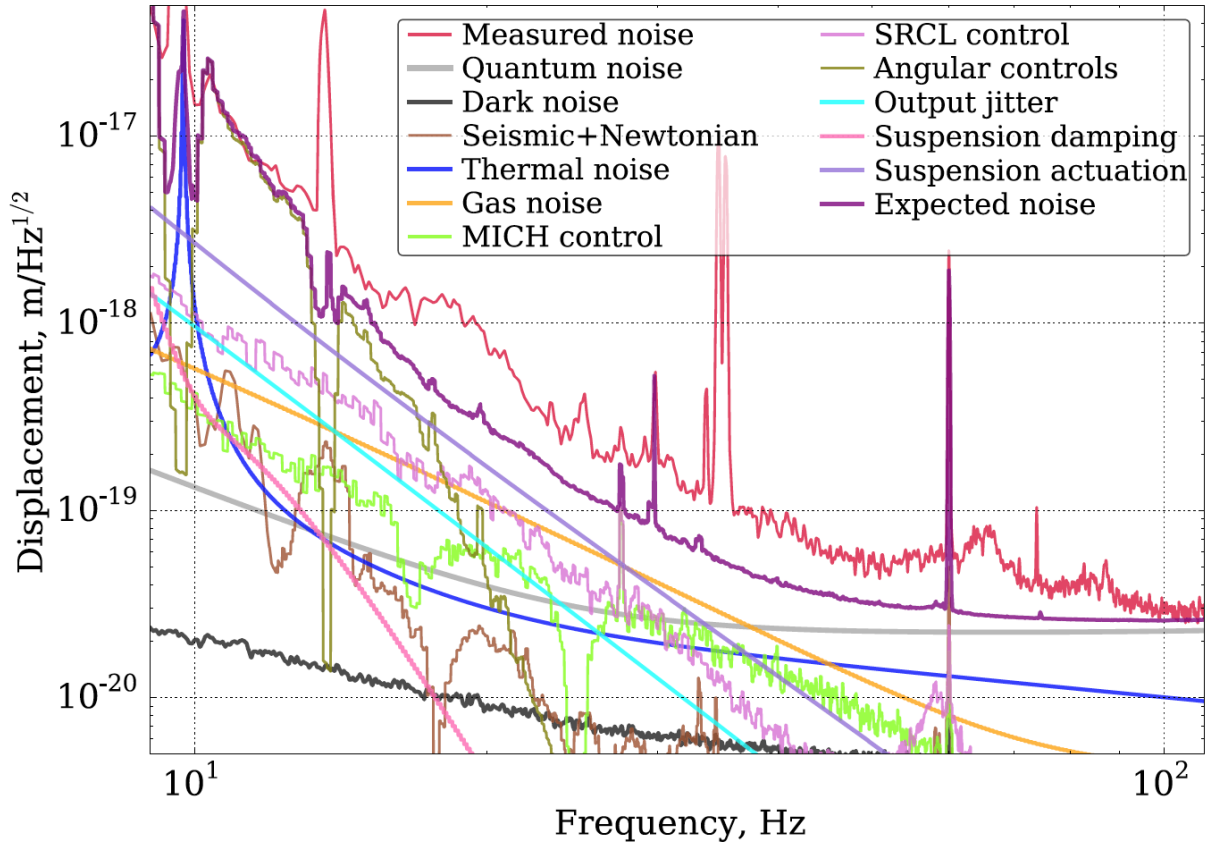


FIGURE 1: Noise budget of aLIGO [1]. In the 10–100 Hz band, the sensitivity is limited by predictable noises (i.e., noises that are not due to quantum or thermal fluctuations) and thus indicates a large room of potential improvement. The 'Expected Noise' trace is the quadrature sum of all budgeted noise sources and 'Measure noise' is the actual output of the LIGO detector.

In Figure 1 we show the noise budget of aLIGO in its first observing run [1]. As can be seen from the plot, aLIGO's sensitivity does not reach its fundamental limit set by the quantum and thermal noises until 100 Hz. In fact, the total noise (the red "Measured Noise" trace in Figure 1) in the 10–20 Hz band the noise is nearly two orders of magnitude above its fundamental limit determined by the quantum (the grey "Quantum Noise" trace) and thermal noise (the blue "Thermal Noise" trace).

Our goal, as illustrated in the flow diagram in Figure 2, is to develop machine-learning-based nonlinear regression techniques to remove the auxiliary channels' contamination to the GW channel, and hence improve the aLIGO sensitivity in the sub – 100 Hz band.

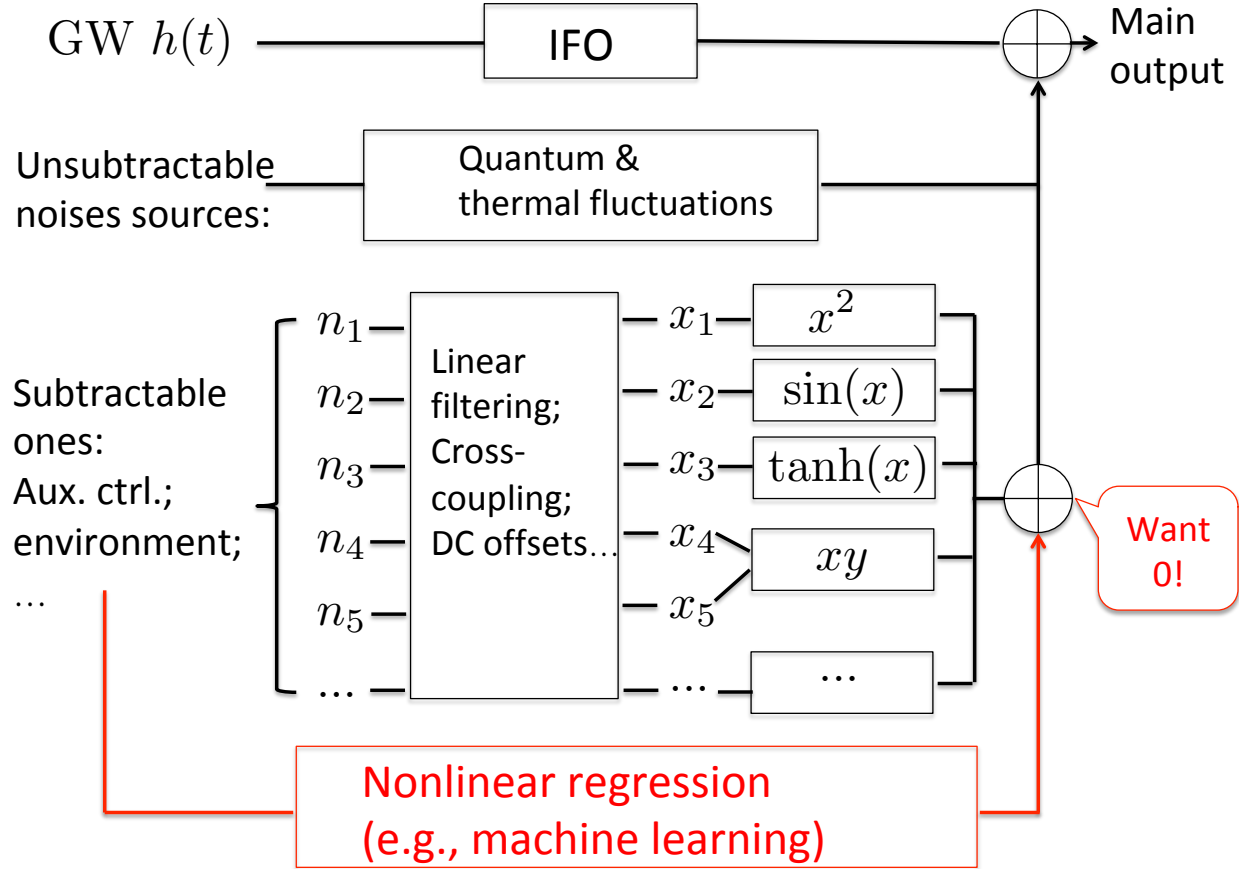


FIGURE 2: Flow diagram of signal and noise propagation. While the original perturbations of the subtractable noises are recorded, identifying their couplings to the main GW readout is challenging. In part, this is due to the large number of channels involved (thousands to tens of thousands). More importantly, the couplings often have both linear and nonlinear components, and hence cannot be removed with classical linear regression methods. Instead, our goal is to develop machine-learning-based nonlinear regression techniques to use time series from the auxiliary channels to construct the disturbance and then remove it from the main GW readout.

2 Examples of Nonlinear Coupling Mechanisms

How a noise source propagates to the main GW readout is often a complicated (and sometimes unknown) process. We show in Figure 3 two examples of typical nonlinear noise coupling that happens in aLIGO.

In the left panel, the angular motion of the mirror and the beam spot motion can couple to create a length signal that mimics the GW. If the beam spot is displaced Δy from the rotational pivot and the mirror is rotated by $\Delta\theta$, it creates a fluctuation in length, ΔL ,

$$\Delta L(t) = \Delta y(t)\Delta\theta(t) \quad (1)$$

where the quantities are defined in Figure 3a. In this case, the contamination is the product of two auxiliary noise sources (LIGO doesn't directly measure Δy but it can be inferred from other channels).

Another important noise is due to backscattering, which is illustrated in the right panel. Because of defects of a mirror's surface, it can scatter off some light from the main beam (in Figure 3b this occurs at the end test mass EX, but it can also occur at other optics). The stray lights may reflect upon some scattering objects (e.g., chamber walls) and recombined to the main beam. This process creates light fields ΔE whose phase is shifted with respect to the main field E_0 by an amount of

$$\frac{\Delta E}{E_0}(t) \propto \exp \left[4\pi i \frac{\Delta x(t)}{\lambda} \right], \quad (2)$$

where λ is the laser's wavelength and $\Delta x(t)$ is the relative displacement between the mirror and scattering objects. When $\Delta x(t) \gtrsim \lambda$, the scattered field $\Delta E(t)$ becomes nonlinear and can up-scatter the large, low-frequency seismic motion into the band of GW readout.

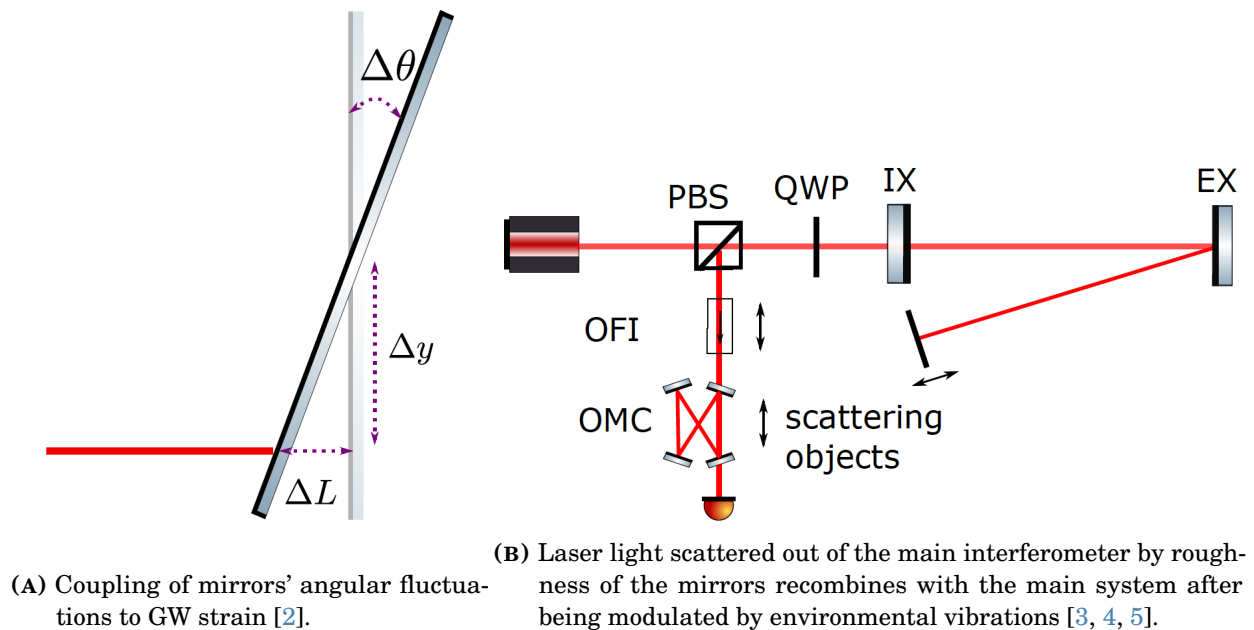


FIGURE 3: Examples of nonlinear noise coupling in LIGO.

3 Noise regression with Neural Networks

Before tackling real data, we simplify the problem by working with mock data sets that mimic the real interferometer. Each of our mock data sets consists of:

- **A target channel**, which is a time-series containing simulated noise in the GW readout, also called DARM in the context of interferometers.
- **Witness channels**, which are the time series necessary to predict the target channel. They correspond to a subset of hundreds to thousands of auxiliary channels in LIGO.

- **A cost function**, which can be either the root-mean-squared (RMS) value of the cleaned DARM time-series, or the power spectral density of DARM with appropriate frequency-dependent weighting.

We increase the complexity of the mock data sets as we have success. Some of the complications built into are mock data sets include:

- **Imperfect witnesses.** Certain quantities like the beam's location on a mirror or the motion of the exact scattering point (as we don't know its exact location), are often not directly measured. Instead, they themselves need to be first inferred from other channels (e.g., the spot location on a mirror may be contained in a combination of seismometers and angular sensors; the motion of the unknown scattering point can be interpolated from a sets of accelerometers nearby).
- **Frequency dependent filtering.** The auxillary channels (which are measured in digital counts) often require linear, frequency-dependent filtering to become physically relevant quantities like the longitudinal or angular motion of the mirror.

We try to find a neural network that can efficiently predict the target channel from the witness channels for all of our mock data sets. So far we have found that

- 1D convolutional neural networks perform well, especially for learning phase shifts and frequency-dependent filtering.
- Dense layers with nonlinear activation functions are useful for learning nonlinear couplings between channels
- Dropout layers are necessary to prevent overfitting.

Besides brute-force deep filtering with a generic nonlinear activation function, a promising direction to further enhance the performance of a neural network is to utilize our knowledge (section 2) of the physical model into the design of the network.

4 Reinforcement Learning for Feedback Controls

1. the LIGO control systems are generally static, linear, and designed 'by hand'
2. the noise below 60 Hz is polluted by noise from these control systems
 - (a) this is mostly due to the angular controls
 - (b) feedback to the Signal Recycling mirror also contributes
3. better feedback/feedforward should be able to reduce this noise
 - (a) possibly through design of a better linear controller
 - (b) more likely through non-linear feedback

A toy example would be an adaptive controller whose control bandwidth is adjusted according to the RMS motion of the input disturbance.
 - (c) nonlinear synthesis of the loop error signal incorporating environmental signals
 - (d) similar to many of the 'Classic Control' problems in the openai framework

4. better and more robust feedback control is necessary if we want to increase the power input to LIGO to reduce its high-frequency shot noise.
5. need to define the cost function correctly
6. LIGO team needs to define the opto-mechanical plant better
7. the control should be performed in a multiple-input-multiple-output sense

A Astrophysical Motivations

Astrophysically, removing the excess noise in the sub-100 Hz band will have significant outcomes, including

- detecting intermediate-mass black holes (IMBHs);
- early-warning of binary neutron star (BNS) mergers;
- constraining binary black hole (BBH) formation channel via eccentricity measurements;
- and many more.

For example, the gravitational-wave signal of a black hole binary has a characteristic frequency scale given by

$$f_{\text{merger}} \simeq 40 \left(\frac{3}{1+z} \right) \left(\frac{100 M_{\odot}}{M_{\text{tot}}} \right) \text{Hz}, \quad (3)$$

where z is the cosmological redshift and M_{tot} is the total mass of the system. Therefore, in order to detect massive binaries (especially those including at least one IMBH) at high cosmological redshifts, it is critical to improve the low-frequency sensitivity that is limited by predictable noises.

More quantitatively, we note that the signal-to-noise ratio (SNR) of a GW event can be written as

$$\text{SNR}^2 = 4 \int \frac{f h^*(f) h(f)}{S_n(f)} d \log f, \quad (4)$$

where $h(f)$ is the frequency-domain GW waveform and $S_n(f)$ is the power spectral density of the noise. We can hence define

$$\rho^2 \equiv 4 \frac{f |h(f)|^2}{S_n(f)}, \quad (5)$$

as a density that measures the contribution to the total SNR per $\log f$.

We show the detection horizon (the distance at which a GW event has an $\text{SNR} \geq 8$ with optimal orientation) as a function of the detector-frame total mass in Fig. 4 (assuming the binary has an equal mass). In order to detect systems with $(1+z)M_{\text{tot}} \gtrsim 300 M_{\odot}$, (which can be intrinsically massive systems involving IMBHs or can be systems at high cosmological redshift), it is critical to improve the low-frequency sensitivity. For a system with total mass of $(1+z)M_{\text{tot}} = 300 M_{\odot}$ in the detector frame, the SNR can be improved by 40% if our machine learning technique eventually cleans contamination in the low-frequency region. This means amplifying the search volume of such systems by a factor of $\sim 1.4^3 \simeq 2.7$.

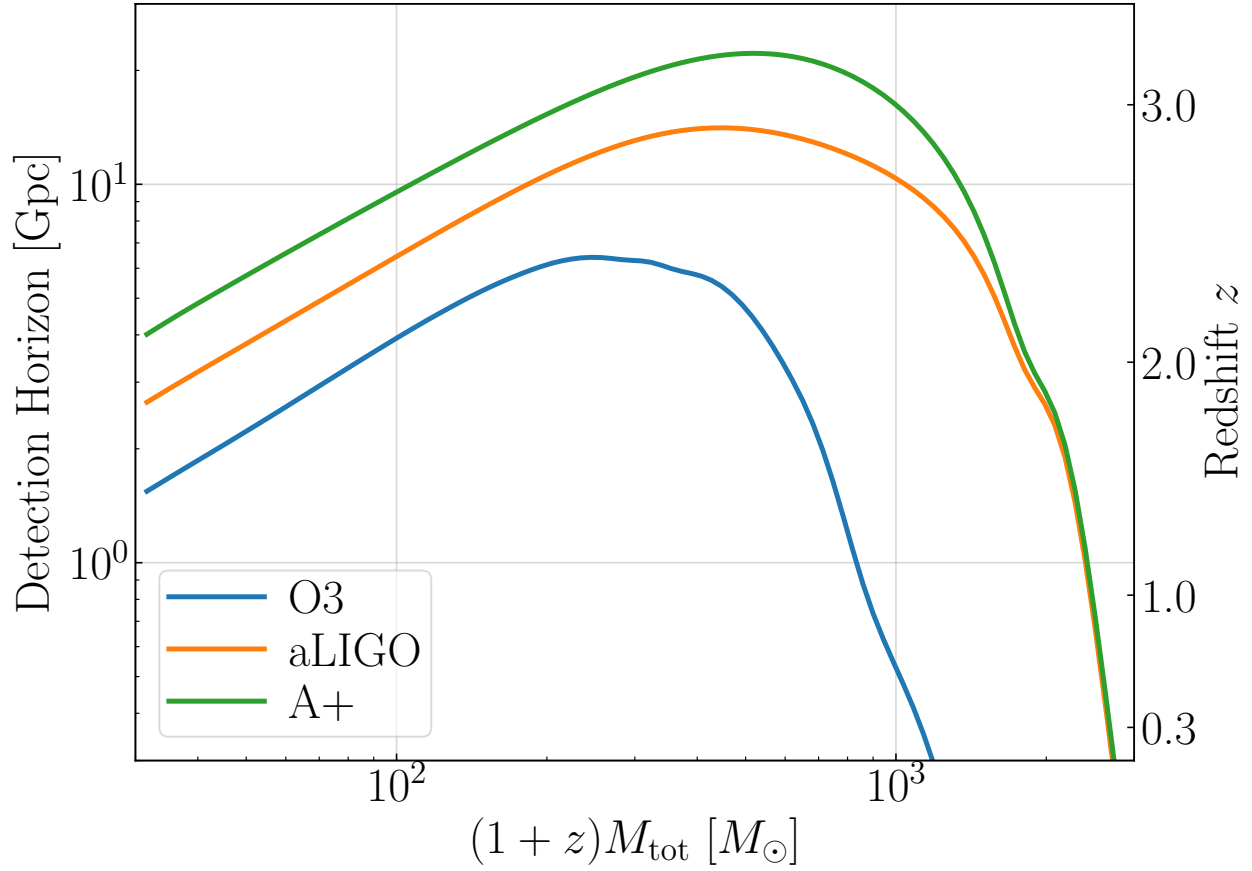


FIGURE 4: Detection horizon as a function of the detector-frame total mass of a binary. Here we further assume the binary has an equal mass. The low-frequency sensitivity plays a crucial role in the detection of systems with $(1+z)M_{\text{tot}} \gtrsim 300 M_{\odot}$.

Enhancing the low-frequency sensitivity also allows us to detect a signal at an earlier time. This is because the time to merger t_m is given by

$$t_m = 87 \text{ s} \left(\frac{\mathcal{M}_c}{M_\odot} \right)^{-5/3} \left(\frac{f}{25 \text{ Hz}} \right)^{-8/3}, \quad (6)$$

where \mathcal{M}_c is the chirp mass of the binary.

In Fig. 5 we show the cumulative SNR as a function of the time to merger t_m . If we can open up the low-frequency window, it means we would potentially be able to catch a BNS signal $\mathcal{O}(100)$ s prior to its final merger [6]. This would allow us to detect not only the post-merger kilonova, but also precursor electromagnetic signals [7, 8, 9, 10, 11].

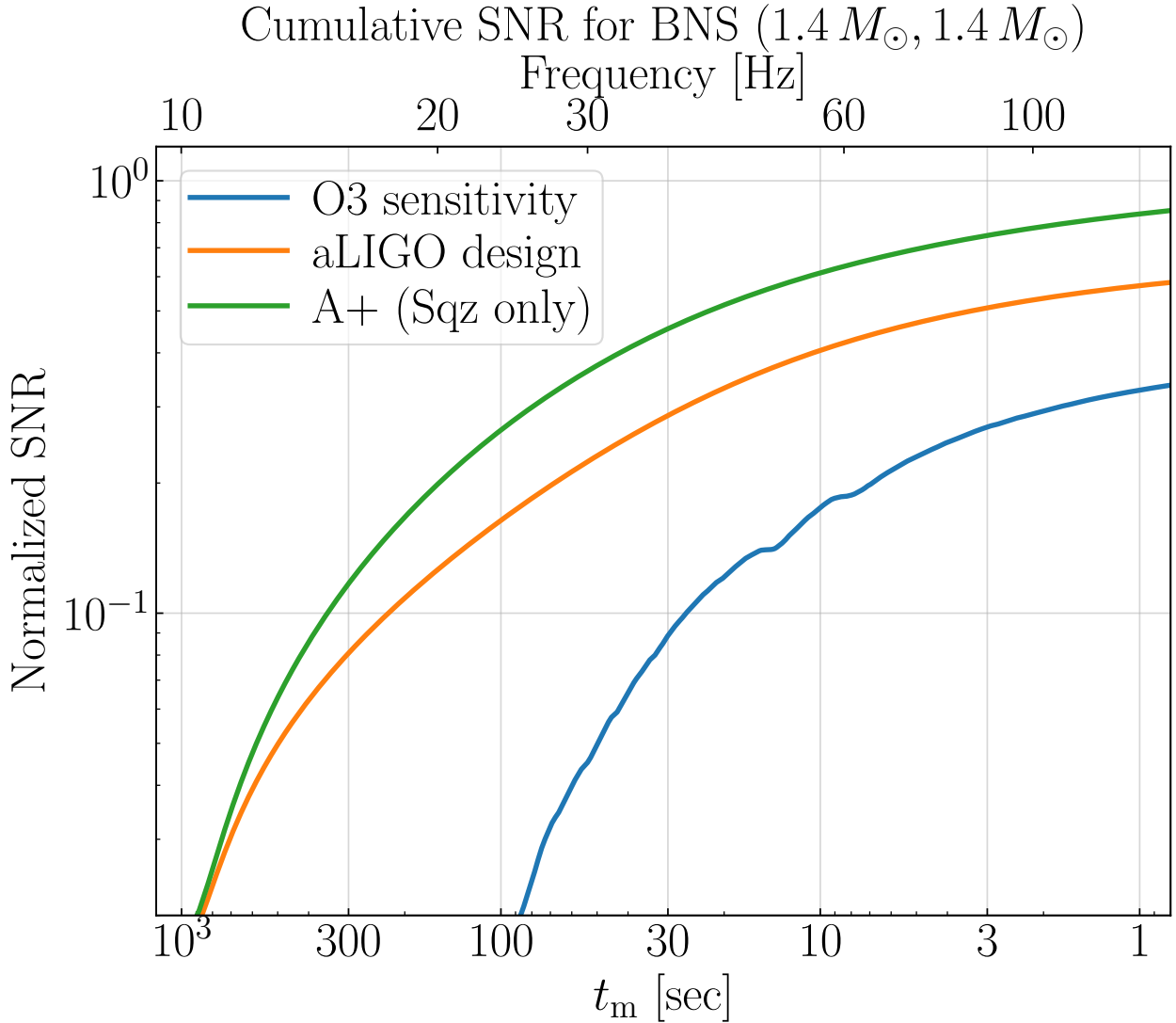


FIGURE 5: Cumulative SNR of a BNS event as function of the time to merger. We also show the corresponding GW frequency in the top x-axis.

Moreover, the sub-100 Hz sensitivity contains valuable information about a BBH's origin. If it is formed via a dynamical channel, it may have small residual eccentricity when it

enters LIGO’s sensitivity band, whereas a BBH formed from an isolated binary should have a circular orbit [12]. Therefore, detecting the a BBH’s eccentricity could serve as a smoking-gun evidence of its formation channel.

In Fig. 6, we compare the characteristic strain of an eccentric BBH with the background instrumental noise [13]. For a circular BBH under the quadrupole formula, the GW emits only via the $n = 2$ harmonic (that is, the GW frequency is twice the orbital frequency). When $e > 0$, the GW can also be emitted via other harmonics (such as the $n = 1$ and $n = 3$ ones shown in the plot). On the other hand, GW radiation is efficient in terms of circularizing the orbit, causing the emission at other harmonics to decay quickly [14]. As a result, detecting $n \neq 2$ harmonics rely critically on the low-frequency sensitivity of the instrument.

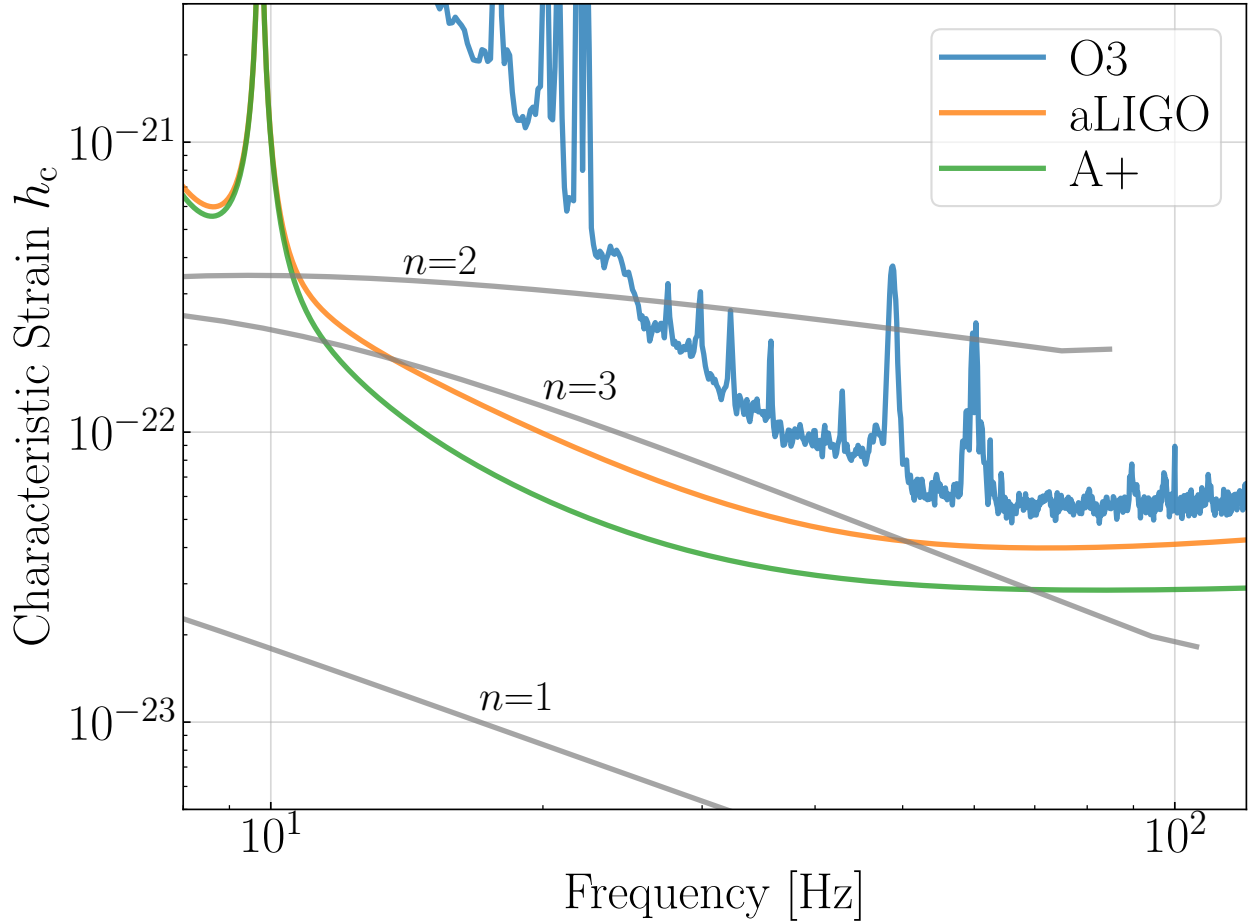


FIGURE 6: Comparison of the characteristic strains of an eccentric BBH merger and the instrumental noise (shown in $\sqrt{fS_n}$). The binary has $M_1 = M_2 = 30 M_\odot$ and an eccentricity of $e = 0.5$ when $f_{\text{orb}} = 1 \text{ Hz}$ and $e = 0.14$ when $f_{\text{orb}} = 5 \text{ Hz}$. Here f_{orb} is the orbital frequency. The evolution is terminated at the inner most stable orbit. In order to detect the eccentricity, one need to detect the harmonics other than the $n = 2$ one.

References

- [1] D. V. Martynov, E. D. Hall, B. P. Abbott, R. Abbott, T. D. Abbott, C. Adams, R. X. Adhikari, R. A. Anderson, S. B. Anderson, K. Arai, and et al. Sensitivity of the Advanced LIGO detectors at the beginning of gravitational wave astronomy. *PRD*, 93(11):112004, June 2016.
- [2] Hang Yu. *Astrophysical signatures of neutron stars in compact binaries and experimental improvements on gravitational-wave detectors*. PhD thesis, Massachusetts Institute of Technology, 2019.
- [3] Denis V. Martynov. *Lock Acquisition and Sensitivity Analysis of Advanced LIGO Interferometers*. PhD thesis, California Institute of Technology, 2015.
- [4] Rana X Adhikari. Integrated detector commissioning. *Advanced Interferometric Gravitational-Wave Detectors*, pages 685–704, 2019.
- [5] S Soni, C Austin, A Effler, R M S Schofield, G Gonzalez, V V Frolov, J C Driggers, A Pele, and et al. Reducing scattered light in LIGO’s third observing run. *arXiv e-prints*, page arXiv:2007.14876, July 2020.
- [6] Hang Yu, Rana X. Adhikari, Ryan Magee, Surabhi Sachdev, and Yanbei Chen. Early warning of coalescing neutron-star and neutron-star-black-hole binaries from the non-stationary noise background using neural networks. *Phys. Rev. D*, 104(6):062004, September 2021.
- [7] David Tsang, Jocelyn S. Read, Tanja Hinderer, Anthony L. Piro, and Ruxandra Bondarescu. Resonant Shattering of Neutron Star Crusts. *Phys. Rev. Lett.*, 108(1):011102, January 2012.
- [8] Brian D. Metzger and Anthony L. Piro. Optical and X-ray emission from stable millisecond magnetars formed from the merger of binary neutron stars. *MNRAS*, 439(4):3916–3930, April 2014.
- [9] Brian D. Metzger and Charles Zivancev. Pair fireball precursors of neutron star mergers. *MNRAS*, 461(4):4435–4440, October 2016.
- [10] Elias R. Most and Alexander A. Philippov. Electromagnetic Precursors to Gravitational-wave Events: Numerical Simulations of Flaring in Pre-merger Binary Neutron Star Magnetospheres. *ApJ*, 893(1):L6, April 2020.
- [11] Zhen Pan, Zhenwei Lyu, Béatrice Bonga, Néstor Ortiz, and Huan Yang. Probing Crust Meltdown in Inspiring Binary Neutron Stars. *Phys. Rev. Lett.*, 125(20):201102, November 2020.
- [12] B. P. Abbott et al. Search for Eccentric Binary Black Hole Mergers with Advanced LIGO and Advanced Virgo during their First and Second Observing Runs. *Astrophys. J.*, 883(2):149, 2019.
- [13] Leor Barack and Curt Cutler. LISA capture sources: Approximate waveforms, signal-to-noise ratios, and parameter estimation accuracy. *Phys. Rev. D*, 69(8):082005, April 2004.

- [14] Hang Yu, Sizheng Ma, Matthew Giesler, and Yanbei Chen. Spin and eccentricity evolution in triple systems: From the Lidov-Kozai interaction to the final merger of the inner binary. *Phys. Rev. D*, 102(12):123009, December 2020.